Vol 17 No 11, November 2008
1674-1056/2008/17(11)/4129-08

Chinese Physics B

© 2008 Chin. Phys. Soc.
and IOP Publishing Ltd

Wavefront depinning in semiconductor superlattices due to discrete-mapping failure*

Wang Jun(王 军) and Zheng Zhi-Gang(郑志刚)†

Department of Physics and the Beijing-Hong Kong-Singapore Joint Center for Nonlinear and Complex Systems (Beijing), Beijing Normal University, Beijing 100875, *China*

(Received 2 February 2008; revised manuscript received 2 April 2008)

We investigate the wavefronts depinning in current biased, infinitely long semiconductor superlattice systems by the method of discrete mapping and show that the wavefront depinning corresponds to the discrete mapping failure. For parameter values near the lower critical current in both discrete drift model (DD model) and discrete drift–diffusion model (DDD model), the mapping failure is determined by the important mapping step from the bottom of branch γ to branch α. For the upper critical parameters in DDD model, the key mapping step is from branch γ to the top of the corresponding branch α, and we may need several active wells to describe the wavefronts.

Keywords: semiconductor superlattice, wavefront depinning, sequential tunnelling
PACC: 0547, 7220H, 7980

1. Introduction

Wavefront propagation failure and fronts depinning (the transition from stationary wavefronts to travelling wavefronts) in the current biased, infinitely long weakly coupled superlattice (SL) systems have attracted much attention in the past years because characterizing the wavefronts travelling under constant current condition is helpful to analysing the self-oscillation under constant dc applied voltage, and the stationary monopoles on finite superlattices basically correspond to the stationary wavefronts of the infinitely long superlattices.[1−4]

For weakly coupled doped semiconductor superlattices, the main mechanism of vertical transport is sequential tunnelling.[1,2,5−10] For different doping values, many interesting phenomena with reference to the negative differential resistance (NDR)[11] have been found in SLs under constant dc applied voltage. For heavy enough doping, a multibranched $I-V$ characteristic is observed due to the formation of two static electric field domains, separated by a domain wall in the form of a charge accumulation layer (CAL), or briefly, a monopole.[12−17] At intermediate doping values, the current self-oscillation appears due to the motion of the domain wall.[18,19] And driven chaotic oscillations have also been predicted and observed in experiment.[20−23]

Starting from a microscopic sequential tunnelling model, the above nonlinear phenomena can be described by discrete balance equations.[24] One widely used simplified model is the discrete drift model (DD model), which was firstly introduced by Bonilla *et al* for electric fields above the first plateau.[3,8] Then for low dc voltage and at low temperature, a discrete diffusion term was added and the DD model turns into the discrete drift–diffusion model (DDD model).[3,4] In these models, the domain wall contains one or several SL periods, and the electric field E_i of the domain wall SL wells are connected to their neighbours (E_{i-1} for DD model and E_{i+1}, E_{i-1} for DDD model) by a discrete mapping. This mapping depends on the doping and current rather than the applied voltage, which merely determines the location of the domain wall.[8,10] Based on this point, we consider an infinitely long, sufficiently doped superlattice system under constant current condition in both DD model and DDD model. The wavefronts in these infinitely long SL systems correspond to the monopole domain walls under voltage biased condition.

*Project supported in part by the State Key Program of National Natural Science of China (Grant No 70431002), the National Natural Science Foundation of China (Grant No 10575010), the National Basic Research Program of China (Grant No 2007CB814805), and the Foundation of Doctoral Training of China (Grant No 20060027009).

†E-mail: zgzheng@bnu.edu.cn

The analysis of the wavefronts motion has been performed by previous researchers.[3,4] In DDD model, the wavefront is pinned for current values in a certain interval $(J_1,\ J_2)$ and depinned when the current surpasses these two threshold currents. The fronts move downstream (the direction of the electron motion) if the current is below J_1 and move upstream (the direction opposite to the flow of the electron) above J_2.[3] In DD model, we obtain only the lower threshold J_c (J_c is slightly larger than J_1) and the wavefronts fail to propagate for $J > J_c$. So the discrete diffusivity or back-tunnelling should be responsible for the emergence of the upstream-travelling wavefronts.[1] Carpio *et al* have explained these critical phenomena based on the comparison principle and estimated the bounds for the critical doping values.[3] However, there is a gap between Carpio *et al*'s bound and the simulation result in the $\nu(J_1)$ curve. For the upper threshold J_2, only the branch for large ν is estimated and it is invalid for small ν.

Our motivation of this paper is to explain the wavefront propagation failure and wavefront depinning on discrete SL systems in terms of discrete mapping and eliminate these gaps. Our paper is organized as follows: The discrete mapping in DD model and its application for explaining the threshold current J_c is presented in the second section. In Section 3, we analyse the discrete mapping failure in DDD model and explain the two critical currents according to our simulation results. Section 4 gives our conclusions and comments.

2. Discrete mapping failure in the DD model

Following the pioneering work on wavefront propagation in semiconductor superlattice systems, we consider the simple discrete drift model for an infinitely long doped SL under the constant current condition in dimensionless form:[3,8,10]

$$\frac{\mathrm{d}E_i}{\mathrm{d}t} + v(E_i)\left(1 + \frac{E_i - E_{i-1}}{\nu}\right) = J(t). \qquad (1)$$

We use the approximate dimensionless coefficient for $v(E)$, given by Ref.[4]. Let $(E_\mathrm{m},\ v_\mathrm{m})$ be the local minimum of $v(E)$ for $E > 1$, and we limit the value of J between v_m and 1 ($v_\mathrm{m} \le J \le 1$) in order to obtain three solutions $E^{(1)}(J)$, $E^{(2)}(J)$ and $E^{(3)}(J)$ ($E^{(1)} \le E^{(2)} \le E^{(3)}$) from the equation $v(E) = J$. Because there are no stationary wavefronts corresponding to charge depletion layer (CDL), so we are interested in the nonuniform wavefronts which satisfy $E_i \to E^{(1)}(J)$ as $i \to -\infty$ and $E_i \to E^{(3)}(J)$ as $i \to \infty$ and these states correspond to CAL: $n_i - 1 = (E_i - E_{i-1})/\nu > 0$.[1,2]

For the stationary state, $\mathrm{d}E_i/\mathrm{d}t = 0$. Then we have a so-called discrete mapping[8] from E_i to E_{i-1}:

$$E_{i-1} = f(E_i; J, \nu), \qquad (2)$$

$$f(E; J, \nu) = E + \nu(1 - \frac{J}{v(E)}). \qquad (3)$$

$v(E) = J$ is equivalent to $f(E) = E$, so we can obtain three intersection points of the curve $f(E)$ with the straight line E versus E at $E^{(1)}$, $E^{(2)}$ and $E^{(3)}$, as shown in Fig.1.

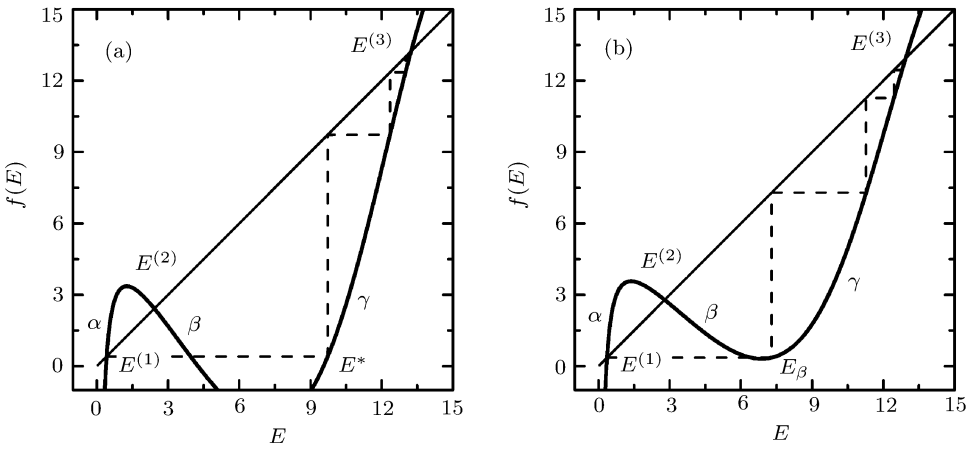


Fig.1. The discrete mapping for $\nu = 3.0$ in DD model. (a) $J = 0.25$ (above the threshold). (b) $J = 0.196$ (around the threshold).

Equation (2) allows us to obtain the whole electric field profile $\{E_i; i = -\infty, ..., \infty\}$, if there do exit such a stationary profile for given J and ν. Let us call branch α that satisfies $\partial f(E)/\partial E > 0$ for lower E, branch β with $\partial f(E)/\partial E < 0$, and branch γ again satisfies $\partial f(E)/\partial E > 0$ but for larger E. There are two points for $\partial f(E)/\partial E = 0$, E_α at the top of the branch α and β as local maximum and E_β at the bottom of the branch β and γ as local minimum value.

For stationary profiles, branch β is crossed by a single jump from $E^{(1)}(J)$ to branch γ, as shown in Fig.1(a). This means that for a certain $E^{(1)}$, there exits such a E^* at branch γ with $f(E^*; J; \nu) = E^{(1)}(J)$. As ν is decreasing, E^* decreases towards E_β, and the necessary and sufficient condition for the exitance of such a jump (mapping step) is

$$f(E_\beta; J, \nu) \leq E^{(1)}(J). \tag{4}$$

If the parameters J and ν do not allow us to perform such a jump from branch γ to α, the wavefronts will be depinned, then we call this case the discrete mapping failure. Equation (4) gives the critical condition of the transition from stationary wavefronts to travelling ones. Figure 2 depicts the critical values of J_c and ν, which satisfy Eq.(4), by the solid line, and solid squares denote the critical current J_c obtained by simulation. They are in good agreement with each other.

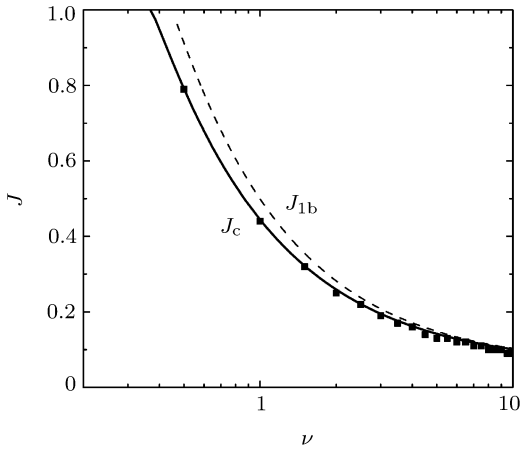


Fig.2. Critical values of J. Solid line denotes critical values of J_c and ν, which satisfy Eq.(4). Solid squares denote the critical current J_c obtained by simulation. Dashed line shows Carpio *et al*'s bound, Eq.(18) in Ref.[3].

For given J and ν, the discrete mapping failure is mainly determined by the shape of the $f(E)$ curve and its derivative is

$$\frac{\partial f(E)}{\partial E} = 1 + J\nu\frac{v^{'}(E)}{v^2(E)}. \tag{5}$$

At the point (E_m, v_m) we have $v'(E_m) = 0$ and $f'(E_m) = 1$, while E_β is the local minimum of $f(E)$, and $f'(E_\beta) = 0$. Because both E_β and E_m are on the branch γ, so $E_m > E_\beta$, and $f(E_m) > f(E_\beta)$. We assume that $f(E_\beta) = f(E_m) + \Delta(\Delta < 0)$. Critical condition Eq.(4) means that

$$\begin{aligned} E^{(1)}(J_c) =& f(E_\beta) \\ =& f(E_m) + \Delta \\ =& E_m + \nu\frac{v_m - J_c}{v_m} + \Delta. \end{aligned} \tag{6}$$

Therefore we obtain

$$\nu = v_m\frac{E_m - E^{(1)}(J_c) + \Delta}{J_c - v_m}. \tag{7}$$

As J_c is increasing, $E^{(1)}(J_c)$ also increases, therefore ν is a decreasing function of J_c according to Eq.(7). On the other hand, we may have

$$\begin{aligned} J_c =& v(E^{(1)}(J_c)) \\ =& v(f(E_\beta)) \\ =& v(f(E_m)) + \left.\frac{\partial v}{\partial E}\right|_{f(E_m)}\Delta, \end{aligned} \tag{8}$$

and furthermore,

$$\Delta = \frac{J_c - v(f(E_m))}{\left.\dfrac{\partial v}{\partial E}\right|_{f(E_m)}}. \tag{9}$$

If we assume that $E_\beta = E_m$, then we obtain

$$\nu_{1b} = v_m\frac{E_m - E^{(1)}(J)}{J - v_m}, \tag{10}$$

which is exact Carpio *et al*'s bound $\nu_{1b}(J)$ (Eq.(18) in Ref.[3], estimated by the comparison principle) for the inverse function of $J_1(\nu)$ in the DDD model. In their estimating analysis, they ignored the diffusion term, so this bound can also be regarded as the bound for $J_c(\nu)$ in the DD model, and we depict its inverse function $J_{1b}(\nu)$ in Fig.2 by the dashed line. As we will show in the next section, $J_1(\nu)$ is slightly smaller than $J_c(\nu)$. However, $J_c(\nu)$ is smaller than $J_{1b}(\nu)$ because of the negative Δ. So the gap is induced by the negative Δ and neglect of the diffusion term. For lower ν, both $(J_{1b} - J_c)$ and $(J_c - J_1)$ increase, and so this bound $J_{1b}(\nu)$ for $J_1(\nu)$ in the DDD model is not so well founded.

As for the upper threshold current $J_2(\nu)$ in DDD model, the comparison principle can only be used for estimating the bound for the increasing branch of J_2 for large ν,[3] and a more reasonable bound for the

whole $J_2(\nu)$ curve is needed. By analysing the discrete mapping failure, we have obtained the exact form for $J_c(\nu)$, and, we will analyse the discrete mapping failure in the DDD model in the next section.

The wavefront (the domain wall separating two electric field domains) moves downstream when $J < J_c$, i.e. $dE_i/dt < 0$. We will explain this by the discrete mapping. Let us assume that $E_{i-1} = E^{(1)}$ and $E_i > E^{(1)}$ at time t. When the parameters J and ν are in the depinning zone (under J_c in Fig.2), the mapping above is not allowed, but we may have a time-dependent discrete mapping, by which E_i can be mapped to $E^{(1)}$,

$$\begin{aligned} f_t(E_i) =& E_i + \nu\left(1 - \frac{J - \frac{dE_i}{dt}}{v(E_i)}\right) \\ =& E_i + \nu\left(1 - \frac{J}{v(E_i)}\right) + \frac{\nu}{v(E_i)}\frac{dE_i}{dt} \\ =& f(E_i) + \frac{\nu}{v(E_i)}\frac{dE_i}{dt} = E^{(1)}. \end{aligned} \tag{11}$$

If the parameters are in the depinning zone, $\forall E_i > E^{(1)}$, the condition (4) is violated and we have

$$f(E_i) = E_i + \nu\left(1 - \frac{J}{v(E_i)}\right) > E^{(1)}. \tag{12}$$

So the second term of Eq.(11) must be negative, then we can obtain directly

$$\frac{dE_i}{dt} < 0. \tag{13}$$

3. Discrete mapping failure in the DDD model and active wells

In this section, we consider the discrete drift–diffusion model (DDD model),[1,3,4] which contains an electron diffusion term,

$$\begin{aligned} &\frac{dE_i}{dt} + v(E_i)\left(1 + \frac{E_i - E_{i-1}}{\nu}\right) \\ &\quad - D(E_i)\left(\frac{E_{i+1} - 2E_i + E_{i-1}}{\nu}\right) = J(t), \end{aligned} \tag{14}$$

here we also use the approximate coefficient for $v(E)$ and $D(E)$ in Ref.[4]. In contrast with the DD model, new solutions and a new critical current are observed, as shown in Fig.3. The wavefronts may move upstream. If the current $J < J_1(\nu)$, the wavefront moves downstream (to the right). Wavefronts are stationary for $J_1(\nu) < J < J_2(\nu)$, and move upstream (to the left) for currents $J > J_2(\nu)$. Obviously, the appearance of $J_2(\nu)$ should be due to the presence of the discrete diffusion term.

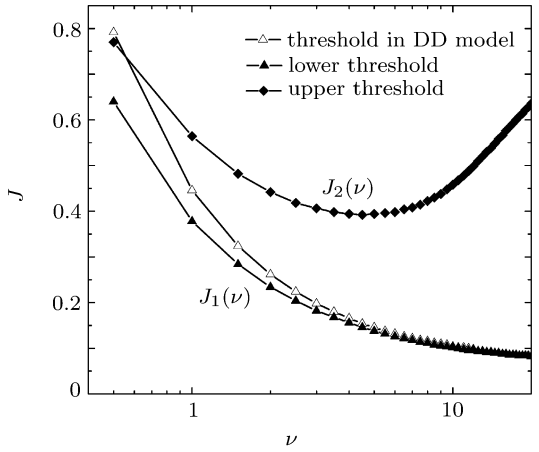


Fig.3. Critical currents as functions of ν in DDD model and comparison with the threshold in DD model.

Analogous to the DD model, we consider the wavefronts propagation failure in DDD model by analysing the discrete mapping on several so-called active wells.[3,4] In the situation of DD model, we may obtain the whole stationary field profile no matter whether the mapping is carried out from E_i to E_{i-1} or from E_{i-1} to E_i, if keeping $E_i \geq E_{i-1}$ (CAL wavefronts). In the DDD model, we also suppose $E_i \geq E_{i-1}$, and mainly consider the mapping from E_i to E_{i-1}.

For the stationary state, $dE_i/dt = 0$, then we obtain

$$E_{i-1} = F(E_i, E_{i+1}; J, \nu), \tag{15}$$

$$\begin{aligned} F(E, E_{i+1}; J, \nu) =& E + \nu\left(\frac{v(E) - J}{D(E) + v(E)}\right) \\ & - D(E)\frac{E_{i+1} - E}{D(E) + v(E)}. \end{aligned} \tag{16}$$

Different from the DD model, the discrete mapping (15) from E_i to E_{i-1} depends on E_{i+1}. So we have to change the $F(E)$ curve for each mapping step. Fortunately, for the first several steps of the mapping on branch γ, the E_i values are close to $E^{(3)}$ (slightly below $E^{(3)}$, as shown in Fig.4), and these $D(E_i)$ values are so small that the third term of Eq.(16) vanishes and we obtain Eq.(3).

In Fig.4, we show part of the discrete mapping steps for $\nu = 3.0, J = 0.1795$ (close to and below $J_1(\nu)$) in (a) and $\nu = 3.0, J = 0.404$ (close to and above $J_2(\nu)$) in (c). The $F(E)$ curves depend on different E_{i+1} given by simulation. The corresponding stationary field profile of (a) and (c) are depicted in (b) and (d).

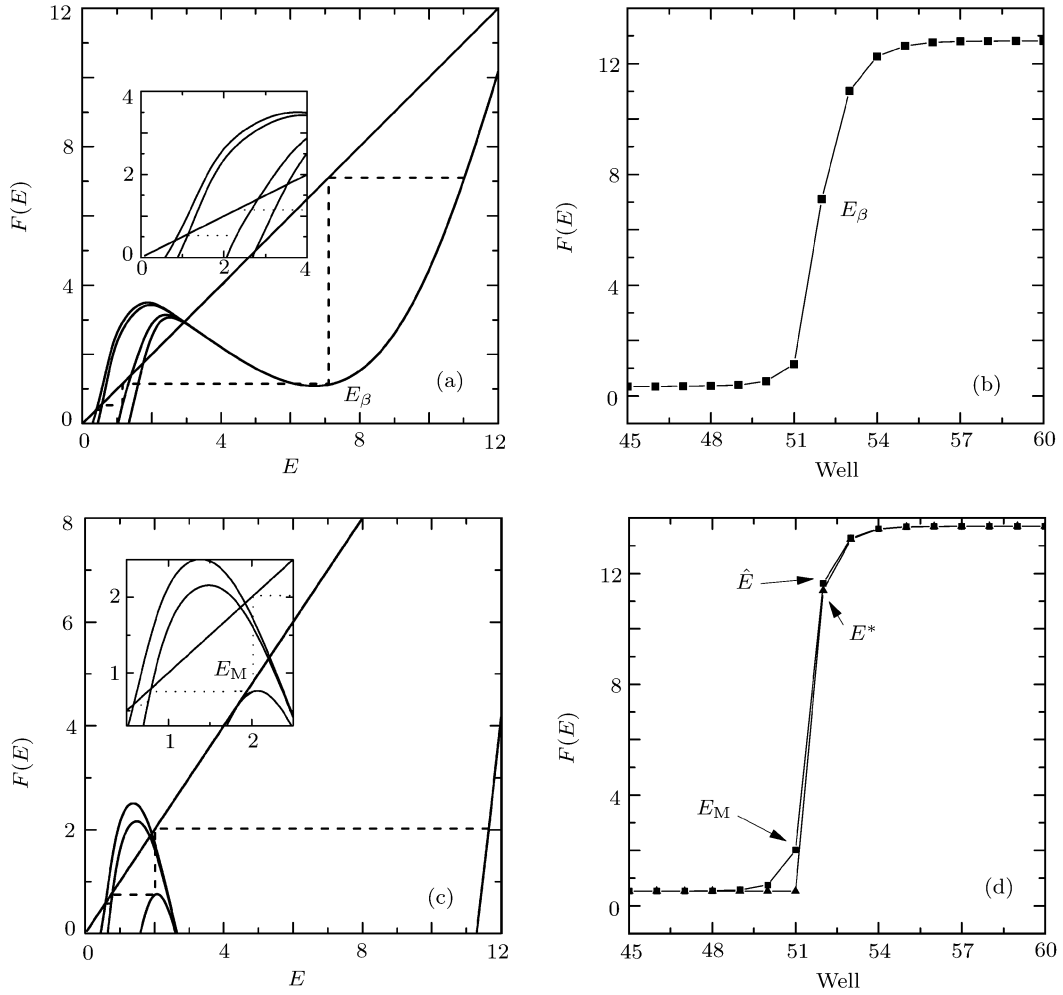


Fig.4. Part of the discrete mapping steps and the corresponding wavefronts profile (denoted by the solid squares) for $\nu = 3.0$ and currents around the threshold currents in DDD model. (a) and (b) for $J = 0.1795$ (around the lower threshold current), (c) and (d) for $J = 0.404$ (around the upper threshold current). The $F(E)$ curves in (a) and (c) depend on different E_{i+1} values given by simulation results. The solid triangles in (d) present the wavefronts in DD model with the same parameters for comparison.

From Fig.4, we find that:

(i) For different E_{i+1}, the branches γ of the curves $F(E)$ almost overlap with each other, and even with the branch γ of the curve $f(E)$ in the DD model owing to small $D(E_i)$.

(ii) Among these mapping steps, the most crucial step to determine the discrete mapping failure is the one from branch γ to branch α, which is mapped to a larger value above $E^{(1)}$, then tends towards $E^{(1)}$ after a few steps, but not to $E^{(1)}$ directly like in the DD model.

(iii) For the parameters around $J_1(\nu)$, this crucial step is similar to the DD model, from E_β to somewhere larger than $E^{(1)}(J)$ in the corresponding branch α, denoted by $E_{\beta-\alpha}$ ($E_{\beta-\alpha} > E^{(1)}$).

(iv) For the parameters around $J_2(\nu)$, the most important step is the one from branch γ to the neighbourhood of the top of the corresponding branch α.

For the case (iii) we have

$$E_{\beta-\alpha} = F(E_\beta, E_{i+1(\beta-\alpha)}; J_1, \nu) \approx f(E_\beta; J_1, \nu) > E^{(1)}(J_1). \quad (17)$$

It means that for the same parameter J_1 and ν in the DD model, the wavefront is depinned. As a results, the lower critical current $J_1(\nu)$ is slightly smaller than the critical current J_c in the DD model due to the presence of the negative diffusion term, as shown in Fig.3.

Next let us analyse the upper critical current $J_2(\nu)$. By comparing between the two profiles in Fig.4(d), we find that there are two special points in the solid square profile (DDD model situation). One

is denoted by $\hat{E}$, which is close to E^* in the solid triangle profile (DDD model situation) with $f(E^*; J, \nu) = E^{(1)}(J)$, and the other one is $E_{\rm M}$.

We suppose that the stationary wavefronts profile in the DDD model is formed in the following way (the first supposition): $E_k = \hat{E}$; $E_{k-1} = E_{\rm M}$; $E_i = E^{(1)}, \forall i < k-1$; and $E_j = E^{(3)}, \forall j > k$. This means that there are only two active wells, $\hat{E}$ and $E_{\rm M}$. The two discrete mapping steps from $\hat{E}$ to $E^{(1)}$ is given by

$$E_{\rm M} = F(\hat{E}, E^{(3)}; J_2, \nu), \tag{18}$$

$$E^{(1)} = F(E_{\rm M}, \hat{E}; J_2, \nu). \tag{19}$$

Based on Fig.4(d) and the point (iv) above, we may give two additional suppositions for these two active wells:

$$\hat{E} = E^*, \tag{20}$$

$$E_{\max} = E_{\rm M} = F(\hat{E}, E^{(3)}; J_2, \nu), \tag{21}$$

here $E_{\max}$ is the local maximum value of the curve $F(E, E^*; J, \nu)$. We have numerically found a number of (J, ν) values which satisfy these three suppositions, and depict them in Fig.5 by the solid triangles. During our simulation, we keep $E_i \geq E_{i-1}$ to obtain the CAL wavefronts.

$D(E) \approx 0$ for large E, so we find no influence of the diffusion term on the mapping steps on the branch γ. But for the mapping steps on the branch α and even the step from branch γ to branch α, we can no longer neglect $D(E)$ any more. According to Eq.(16), the branch α of the curve $F(E)$ is below the curve $f(E)$ for the same parameters due to the negative diffusion term. So when we map from branch γ toward branch α, we always obtain a larger E than $E^{(1)}$, and then the mapping tends to $E^{(1)}$ after a few mapping steps on several active wells. For large ν, the infinitely long, current biased SL systems are in strongly discrete limit.[4] Hereby we need only a few active wells to describe the wavefronts, so the critical current $J_2(\nu)$ and the solid triangle match well with each other in Fig.5 for large ν. For low ν, we obtain the continuum limit, and the influence of the diffusion term is strengthened, more and more wells become active.[4] So our results (the solid triangle in Fig.5) are not so well matched for lower ν.

To improve our predictions, we have to increase the number of active wells. Besides $E_{\max}$ and $\hat{E}$, we introduce two additional active wells: E^{**} (after $\hat{E}$) and $\tilde{E}$ (before $E_{\max}$). These four active wells satisfy

$$F(E^{**}, E^{(3)}; J_2, \nu) = \hat{E}, \tag{22}$$

$$F(\hat{E}, E^{**}; J_2, \nu) = E_{\max}, \tag{23}$$

$$F(E_{\max}, \hat{E}; J_2, \nu) = \tilde{E}, \tag{24}$$

$$F(\tilde{E}, E_{\max}; J_2, \nu) = E^{(1)}(J). \tag{25}$$

We have done the same numerical simulation with these four active wells, and the results are depicted in Fig.5 by the solid circles. They are in good agreement with the upper threshold current $J_2(\nu)$. The existence of four active wells is a good supposition for the infinite SL systems, as shown in Ref.[4].

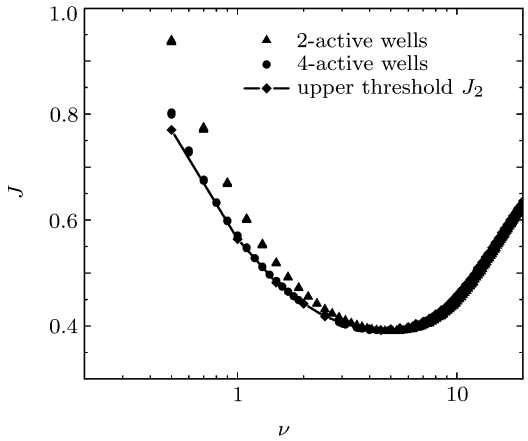


Fig.5. The solid diamond represents $J_2(\nu)$ in Fig.3. The solid triangles and circles denote the (J, ν) values satisfy our suppositions with two and four active wells respectively.

4. Conclusions and comments

We have analysed the wavefront depinning by the method of discrete mapping in both DD model and DDD model of the nonlinear charge transport in current biased, infinitely long superlattice systems. For given values of parameters J and ν, the stationary wavefront corresponds to the realizable mapping from $E^{(3)}$ to $E^{(1)}$ on the curve of $f(E)$ or $F(E)$. If the parameters fall on the critical points where these mappings turn unrealizable (discrete mapping failure), we will obtain the wavefront depinning.

It is much easier to find this critical point in DD model, just given by the mapping step from the bottom of branch γ to $E^{(1)}$. In DDD model, the situation for the lower threshold current is similar to the DD model, but it is complicated for the emergence of the upper threshold current. Firstly, we have to change the curve $F(E)$ for every mapping step. On the other

hand, we need more active wells to characterize the wavefronts. We have simplified this by catching the key mapping step, the step from branch γ to the top of corresponding branch α.

Although the method of discrete mapping cannot be used here to determine the exact form of $J_2(\nu)$, and the stationary wavefront profiles have to be determined numerically, it is effective and encouraging to investigate the wavefront depinning phenomenon in SL systems, and even in other spatially discrete systems, by the discrete mapping. Further more, we are looking forward to finding some physical reality in these discrete systems from the viewpoint of discrete mapping failure.

As we have pointed out above, understanding the motion of the wavefronts is the key to understanding more complex phenomena related to the dynamics of electric field domains. Provided that the charge inside the SL is large enough ($\nu \to \infty$), $J_1 \to v_{\rm m}$ and $J_2 \to 1$, we always obtain stationary states on a finite SL with their domain walls located in one of the SL wells corresponding to one branch of the multi-branched $I-V$ characteristic curve. The location of the domain wall depends on the voltage bias condition. For any branch of the $I-V$ curve, the current increases with voltage bias, but cannot exceed the interval (J_1, J_2). At intermediate doping, the current self-oscillation appears. The current has to oscillate under threshold J_1 to keep on moving downstream.

The upstream-moving wavefronts can be observed in simulations of the SL system under current biased condition at large enough level (above $J_2(\nu)$). And the simulation results confirm our prediction above. It is difficulty to observe the upstream-moving wavefronts in real experiment due to some technical problems.[3] But in the domain wall relocation experiments, we may obtain this phenomena for a short time.[3,15,16] These experiments investigated the transition process from one current branch of the $I-V$ characteristic to the next branch by adding a bias step with different amplitude to the dc bias and recording the time resolved current.[16] After the voltage is suddenly increased, the current response has a sharp peak $I_{\rm p}$, which is much larger than the initial current because of the positive displacement current. For appropriate voltage step, $I_{\rm p}$ may exceed the corresponding threshold current J_2, and the wavefronts move upstream until the current drops below J_2.

Acknowledgment

The authors thank Professor Wang Jian-Nong at Hong Kong University of Science and Technology for initiating the subject.

References

[1] Bonilla L L 2002 *J. Phys.: Condes. Matter* **14** 341
[2] Bonilla L L and Grahn H T 2005 *Rep. Prog. Phys.* **68** 577
[3] Carpio A, Bonilla L L, Wacker A and Schöll E 2000 *Phys. Rev.* E **61** 4866
[4] Carpio A, Bonilla L L and Dell'Acqua G 2001 *Phys. Rev.* E **64** 036204
[5] Esaki L and Tsu R 1970 *IBM J. Res. Dev.* **14** 61
[6] Wacker A 2002 *Phys. Rep.* **357** 1
[7] Platero G and Aguado R 2004 *Phys. Rep.* **395** 1
[8] Bonilla L L, Galán J, Cuesta J A, Martinez F C and Molera J M 1994 *Phys. Rev.* B **50** 8644
[9] Esaki L and Chang L L 1974 *Phys. Rev. Lett.* **33** 495
Grahn H T, Haug R J, Müller W and Ploog K 1991 *Phys. Rev. Lett.* **67** 1618
Kwok S H, Merlin R, Grahn H T and Ploog K 1994 *Phys. Rev.* B **50** 2007
[10] Wacker A, Moscoso M, Kindelan M and Bonilla L L 1997 *Phys. Rev.* B **55** 2466
[11] Sibille A, Palmier J F, Mollot F, Wang H and Esnault J C 1989 *Phys. Rev.* B **39** 6272
Lei X L, Horing N J M and Cui H L 1991 *Phys. Rev. Lett.* **66** 3277
[12] Kastup J, Grahn H T, Ploog K, Prengel F, Wacker A and Schöll E 1994 *Appl. Phys. Lett.* **65** 1808
[13] Grahn H T, Schneider H and von Klitzing K 1990 *Phys. Rev.* B **41** 2890
[14] Bonilla L L, Escobedo R and Dell'Acqua G 2006 *Phys. Rev.* B **73** 115341
[15] Amann A, Wacker A, Bonilla L L and Schöll E 2001 *Phys. Rev.* E **63** 066207
[16] Rogozia M, Teitsworth S W, Grahn H T and Ploog K H 2002 *Phys. Rev.* B **65** 205303
[17] Wu B Y, Duan S Q and Zhao X G 2004 *Chin. Phys.* **13** 1544
Tian Q and Ma B K 1999 *Acta Phys. Sin.* **48** 2125 (in Chinese)
[18] Kastrup J, Hey R, Ploog K H, Grahn H T, Bonilla L L, Kindelan M, Moscoso M, Wacker A and Galán J 1997 *Phys. Rev.* B **55** 2476
Sanchez D, Bonilla L L and Platero G 2001 *Phys. Rev.* B **64** 115311
Sanchez D, Moscoso M, Bonilla L L, Platero G and Aguado R 1999 *Phys. Rev.* B **60** 4489
[19] Wang X R and Niu Q 1999 *Phys. Rev.* B **59** R12755
Wang X R, Wang J N, Sun B Q and Jiang D S 2000 *Phys. Rev.* B **61** 7261

Wang J N, Sun B Q, Wang X R, Wang Y Q, Ge W K and Wang H L 1999 *Appl. Phys. Lett.* **75** 2620

[20] Zhang Y, Kastrup J, Klann R, Ploog K H and Grahn H T 1996 *Phys. Rev. Lett.* **77** 3001

[21] Luo K J, Grahn H T, Ploog K H and Bonilla L L 1998 *Phys. Rev. Lett.* **81** 1290

[22] Bulashenko O M and Bonilla L L 1995 *Phys. Rev.* B **52** 7849
Luo K J, Grahn H T, Teitsworth S W and Ploog K H 1998 *Phys. Rev.* B **58** 12613
Sanchez D, Platero G and Bonilla L L 2001 *Phys. Rev.* B **63** 201306(R)
Cantalapiedra I R, Bergmann M J, Bonilla L L and Teitsworth S W 2001 *Phys. Rev.* E **63** 056216
Lopez R, Sanchez D and Platero G 2003 *Phys. Rev.* B **67** 035330
Sun Z Z , He H T, Wang J N, Wang S D and Wang X R 2004 *Phys. Rev.* B **69** 045315

[23] Amann A, Schlesner J, Wacker A and Schöll E 2002 *Phys. Rev.* B **65** 193313
Amann A, Peters K, Parlitz U, Wacker A and Schöll E 2003 *Phys. Rev. Lett.* **91** 066601
Hizanidis J, Balanov A, Amann A and Schöll E 2006 *Phys. Rev. Lett.* **96** 244104

[24] Bonilla L L, Platero G and Sanchez D 2000 *Phys. Rev.* B **62** 2786